STUDY OF COLLOIDAL LEAD SULFIDE QUANTUM DOT LIGHT-EMITTING-DIODES WITH INORGANIC CHARGE INJECTION LAYERS AND LIGAND EXCHANGES

A Thesis

Presented to the Faculty of the Graduate School

of Cornell University

in Partial Fulfillment of the Requirements for the Degree of

Master of Science

by

Yida Lin

Aug 2014

ABSTRACT

Colloidal quantum dots (CQD) of the IV-VI semiconductor Lead Sulfide (PbS) have shown great potentials in optoelectronic applications such as solar cells and light emitting diodes (LED) in the infrared range. As for LEDs, over 1% external quantum efficiency (EQE) has been achieved with hybrid charge injection layers and PbS quantum dots capped with organic molecules[1]. Here in this thesis, we present our work on PbS quantum dot LED with both inorganic charge injection layers, under several different surface treatment conditions. The thesis begins with the fundamentals on PbS quantum dots including band structures, optical behaviors, surface treatments, etc.. The basics of CQD-based devices will also be introduced. The major part is focused on the fabrication and characterization of LEDs, with the experimental results of the device performance and relevant analyses , followed by the discussion of limiting factors of the performance of LEDs. In the last part, we propose some possible improvements to the device and future concerns.

BIOGRAPHICAL SKETCH

Yida Lin earned his Bachelor of Science degrees in both Physics and Economics at Peking University in 2012. He joined the Master of Science program of the Applied and Engineering Physics at Cornell University in Aug.2012.

Here at Cornell, he has been working on the study of colloidal lead salt quantum dots and related applications since last Sept.. He turned to work on the fabrication of PbS quantum dot LEDs in Feb, 2014, hoping to produce high-efficiency devices for practical applications, and is expecting his degree conferral in Aug based on this research. In the meantime, he developed a great interest in semiconductor technologies on nanoscales, and get familiarized with various kinds of advanced modern fabrication techniques used by industries.

ACKNOWLEDGEMENTS

I would like to give my special thanks to Jun Yang, who helped me very much in acquiring solid understanding of theories and models as well as handling experiements; Haitao Zhang, for all the lab affairs and sample preparation; David Moore, who walked me through important and practical facts in fabrications and tests; Saravanan Rajendran and Ashwin Murthy, for the detailed guidance in fabrication procedures when I just started; Prof. Frank Wise and Prof. Tobias Hanrath, for leading me into this amazing field, and especially, all the patience and help on the last days before the deadline.

TABLE OF CONTENTS

LIST OF TABLES

LIST OF FIGURES

CHAPTER 1

INTRODUCTION AND BACKGROUNDS

1.1 Basics of lead salt colloidal quantum dots

Quantum dots, or known as semiconductor nanocrystals, are made of materials sufficiently small in three dimensions that electrons (or holes) are confined spatially and thus exhibit related quantum-mechanical electronic and optical properties. While charge carriers in conventional bulk semiconductor materials are distributed continuously inside the conduction and valance band separated by the bandgap, they can only sit on discrete energy levels across the original bandgap in quantum dots. The simplest model of quantum dots can be described as "particles in a box", whose energy eigenstates can be solved from basic quantum mechanics. For an ideal spherical spatial confinement, the nth energy level below the valance band edge or above the conduction band is $E_n = \hbar^2\pi^2n^2/2ma^2$, where a denotes the radius and m is the effective mass of the corresponding band respectively. Simple and rough as it is, this relation still shows one principle of the energy levels of quantum dots: the "real" bandgap, which is now the separation between HOMO and LUMO, increases as the dots become smaller, and is always greater than the bandgap of the bulk material.

Although accurate description of energy levels of quantum dots can be rather complicated, satisfactory models have been obtained with the help of envelope functions, k·p theory, etc.. For IV-VI spherical quantum dots PbS and PbSe, the four-band envelope function formalism [2] has been proved to provide accurate energy levels of most states as well as the interband transition strengths and selection rules. This model suggests that both the lowest electron

state and highest hole state are doubly degenerate at each L point (the fcc lattices of PbS and PbSe crystals have 4 equivalent L points) and direct transitions via photon absorption or emission are allowed between all LUMOs and HOMOs. The distinctive result of such discrete energy states is the presence of exciton peaks in both the absorption and photoluminescence(PL) spectra, and in some cases it is even possible to see the second exciton peak corresponding to the 2^{nd} lowest transition in absorption spectra. A typical absorption spectrum of PbS Quantum Dots is shown in Fig.1.1.

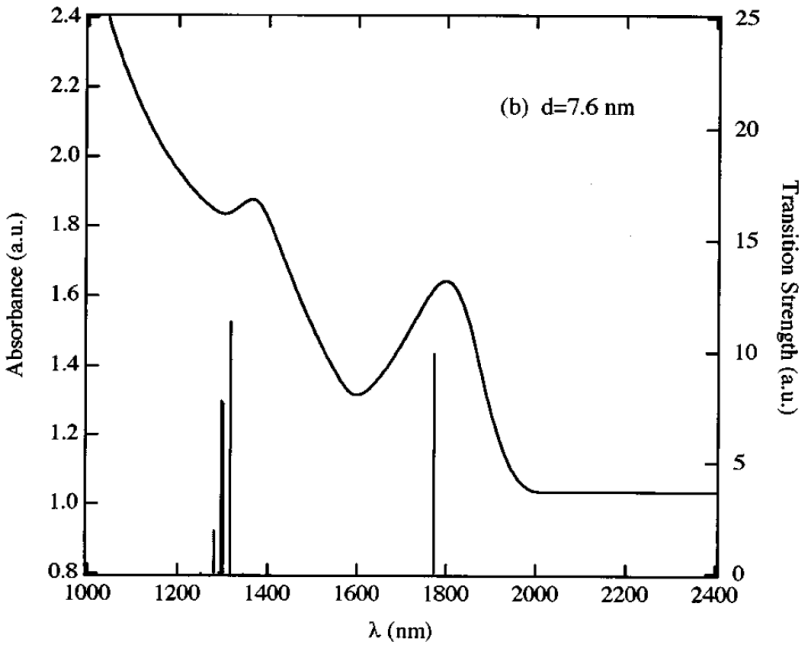

Figure 1.1: [1].Absorption spectrum of 7.6 nm diameter quantum dots. Straight lines are transition strengths calculated with four-band envelope function formalism.

The exciton peaks in the absorption and emission spectra of quantum dots which give rise to their promising properties for optoelectronic applications though, are not unique to PbS and PbSe QDs. The merits of colloidal lead chalcogenide QDs are mainly reflected in the following aspects. First, they are representative of a "strong confinement"[3] regime, where the exciton Bohr Ra-

dius is much larger than that of QDs themselves, and this will enhance greatly the linear and nonlinear resonant optical properties. Also this strong confinement is able to add energy spacing even larger than the original bandgap of PbS or PbSe around 0.2-0.4 eV, to bring about a wide resonance tunability by size from 600 nm-2000 nm, which meets the growing demands for near-infrared emitters and high conversion efficiency solar cells. Another great advantage of colloidal PbS and PbSe QDs lies in the ease of synthesis and handling as well as integration with other structures, based on their solution-processed properties, which compared to materials using epitaxy, such as III-V QDs, is much more convenient and less costly.

1.2 Basics of energy relaxation in PbS QDs

Optical properties of QDs are closely associated with behaviors of electron-hole pairs or "excitons". Specifically, the forming and relaxation of excitons in QDs, is essential to the principles of both solar cells and LEDs. The details of dynamics can be rather complicated and different among QDs of various materials and chemical treatments and the absorption process is generally considered "instantaneous " on timescales of interest while the relaxation dynamics is the main focus of most researches. Here we will give some basic introduction and description of relaxation processes.

Upon absorption of photons, excitons are formed on energy levels with separation equal to the incident photons. The excitons will finally lose their energy and go to the ground states by a variety of pathways occurring in sequence or simultaneously. The major pathway of interest in LEDs is the radiative de-

cay, through which each exciton emits a photon and lands in the ground state. However, the emission photon energy is always not equal to the excitation energy and is usually lower. Apart from Stokes shift [4], a redshift around 100 meV, the difference of energies between excitation and emission results from the fast early intraband relaxations of excitons, where initially formed electron-hole pairs at high energy levels will relaxed into the lowest excited states, i.e. band edge states [5][6]. Despite the complexity of the mechanisms of intraband carrier relaxation which may range from defect-assist transition, to Auger e-h pair interaction [5], the process in most cases is the fastest of all with a picosecond timescale and thus happens before any interband transitions.

The radiative decay of excitons sitting at the band edge, is comparatively easy to understand. For PbS QDs, the process usually has a timescale of few hundred nanoseconds to microsecond. The this type of recombination, accompanied with the depopulation of excitons, can be characterized by transient photoluminescence (PL) spectra, where the time-resolved photoluminescence at given wavelengths are recorded, whose remaining intensity is proportional to the population of existing excitons at the corresponding energy. Another important, or sometimes even more dominant factor of depopulation of excitons is nonradiative interband transitions. The mechanism of nonradiative decay is usually understood as a process assisted by mid-gap trap states without emission of photons.The origin and nature of mid-gap trap states are not fully discovered yet. Most believe trap states are induced more by surface defects or dangling bonds than by the intrinsic property of QDs and therefore surface treatments will have substantial effects on nonradiative decay dynamics [7][8]. The timescales of nonradiative decay revealed in transient PL spectra are usually shorter than radiative recombination and can be as small as few nanosec-

onds [7]. The competition between radiative and nonradiative recombination in PbS QD is one of the most critical concerns for the performance of LEDs.

The radiative recombination rate, which can be theoretically calculated by oscillator strength, in most cases is a constant given the property and status of a QD. But this rate could vary among different initial states of excitons. Because in most conditions of operating devices, the excitement or current injection intensity usually leads to an average number of excitons per QD below unity, the most common radiative recombination rate thus corresponds to a single exciton state, the most probable state in an excited QD, which only consists of one electron in the conduction band and one hole in the valence band. There can be multi-exciton states with faster radiative decay in a QD, allowed by the degeneracy and caused by high injection level . The relationship between this rate and the corresponding exciton state is rather straightforward. It is approximately proportional to the total number of possible pathways, which is the product of number of electrons and holes within the particular QD, i.e. $r_{em} \propto N_e N_h$ [5][9]. For example, a trion (an exciton with an extra hole or electron) has a radiative recombination rate twice of a single exciton and biexciton has a fourfold rate.

The faster recombination rate of multi-exciton states, however, does not render them preferable for applications based on emissions. This is because the existence of extra carriers allows Auger recombination through which the energy from one exciton transfers to another carrier, and will eventually be dissipated to lattice vibration. Auger recombination is undesirable for emitters in that the process is much faster than that of the radiative recombination of any exciton state. Typically, the lifetime is less than 1 ns [9] in PbSe QDs, which leaves almost no chance for radiative recombination before multi-exciton states change

to single-exciton states and for charged exciton states which consist of imbalanced electrons and holes, photon emission can be neglected. Fig.1.2 describes general processes for non-single exciton recombination.

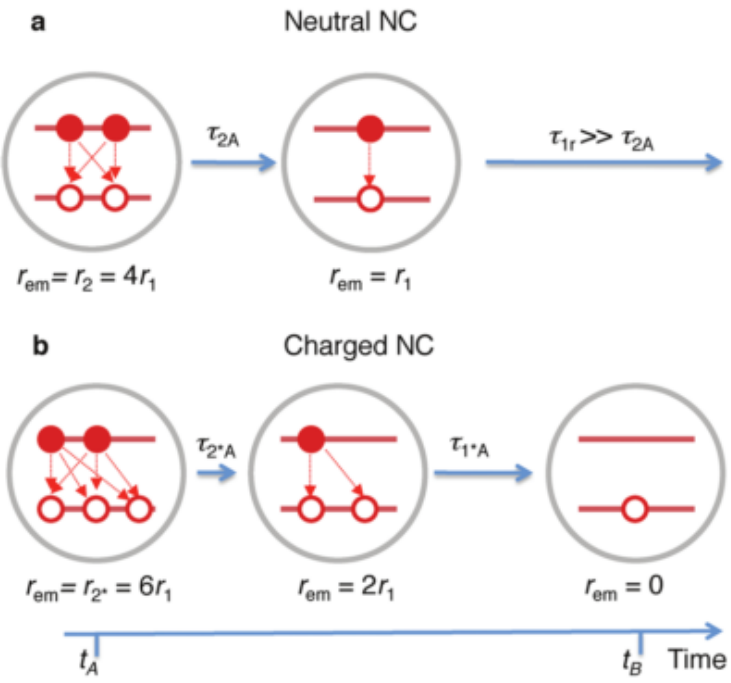

Figure 1.2: [9] Recombination events for (a) biexciton state and (b) biexciton state with an extra hole. r_{em} denotes the radiative recombination rate and every τ denotes the time constant for corresponding radiative or Auger recombination.

1.3 Interactions of coupling QDs

The processes mentioned in the last section apply to QD solutions or QDs dispersed in polymer matrix, where dots are far apart from each other and all the processes can be treated individually. This is not the case for a deposited QD film which is integrated in solar cells and LEDs. On a condensed film, QDs are only separated by the ligands that link to the QD surface at least from one end. And the distance can then become comparable to the diameter of QD or

even smaller. In this regime, the QDs are coupled to each other and interactions for carriers are made possible. The two major processes of interactions are fluorescence resonant energy transfer (FRET) [10][11] and exciton dissociation. The FRET refers to energy transfer from a higher energy exciton on one QD to a nearby QD to generate usually a lower energy exciton, without emission or reabsorption of photons. Because a practical ensemble of QDs always has a distribution of sizes, FRET can occur between smaller dots (higher energy) and larger dots. The time constant of this process can be calculated by $\tau = \tau_d(\frac{R}{R_0})^6$, where τ_d is the radiative recombination life time of the donor and R_0 is the FRET effective radius and is estimated to be around 8 nm [10] for PbS QDs. Due to the sixth power in the relation, the process can be much faster than radiative recombination for closed packed dots with inter-dot distance slightly shorter than 8 nm, which is the case for most PbS dots capped with organic ligands or treated inorganically.

The FRET represents the exciton transfer as a whole while exciton dissociation is the process where individual electron or hole transfers to the nearby acceptor not necessarily in the same direction. The understanding of mechanism of dissociation is still obscure but most believe this is a type of tunneling [7][12], akin to the transfer of electrons between two potential wells of identical energy levels when they come close to each other and an interaction energy is established. The timescale of this process is also significantly ruled by the inter-dot distance and shorter distance facilitates the dissociation exponentially, which is believed to be even faster than FRET when QDs are arranged very closely. An important property of dissociation is that it is able to accumulate charges and generate currents by diffusion or by electric field, which play critical roles in QD-based applications, especially for solar cells, where the carrier diffusion

efficiency largely determines the overall efficiency of the device.

These interactions of coupling QDs, on the other hand, can significantly affect the PL properties of QD assemblies. Unlike isolated QD ensembles where the total emission behavior is simply the sum of that of each individual QD, in close-packed ensembles both the PL dynamics and overall intensity will be strongly modified, and usually appear with lower Quantum Yield (QY) and faster exciton decay. In addition, the FRET will cause a redshift of the emission compared with that in solutions as well as rises in the initial transient PL traces on the red side, simultaneously with falls on the blue side. On the other hand, the exciton dissociation is more detrimental to the PL despite that it promotes charge transfers through QD arrays. The observed transient PL of dissociation- dominated films usually has much shorter effective lifetimes than isolated QD samples and a significant decline in QY. Although there is no doubt that there should be more excitons ending up in nonradiative recombination in a dissociation-dominated regime, in order to account for the decrease in emission compared to uncoupling samples, the exact dynamics of a complex mixture of individual QD behaviors and inter-dot interactions is not fully uncovered. There will be some discussion on this in the last chapter of the thesis.

1.4 Surface treatments and ligands exchanges

The fact that quantum dots are so small with a large surface-to-volume ratio suggests the importance of surface properties to them. The bare surface of a PbS QD will lead to excess dangling bonds and defects that can severely undermine all the merits in optical and electronic properties. As a matter of fact, QDs in

almost every sample, for whatever purpose they are studied, are passivated with ligands or covered with a shell of different material to enhance the surface property. While most are aimed at fixing the surface traps, some of the surface modifications can also considerably modify the major emission properties.

Capping surfaces with organic molecules are widely used for PbS QDs. The treatment is always completed by exchanging the original long chain oleic acid molecules on as-synthesized QDs with shorter chains with thiol or carboxylic function groups. Besides capping the dangling bonds at the surface, these ligands exchanges can be used to tune the inter-dot spacing in close-packed QD films (Fig.1.3)[1][7], which will result in significant variation in exciton dissociation rates.

Another major type of surface modification, to cover the surface of core with a different material, gives rise to the "core-shell" structure QDs. The shell usually consists of a wider bulk bandgap material with matching lattice to the core. Commonly seen core-shell QDs are CdS/CdSe, CdSe/ZnS, PbSe/PbS, PbS/ZnS. The first consequence of the structure is a slightly lower exciton energy compared with the core-only QDs of the same core size. This is because rather than the infinite barrier in core-only structures, the finite barrier from the shell material that carriers feel, allows their wavefunctions to expand outside the core, which corresponds to a slightly larger effective confinement size, and hence lower energy. In addition to a usually higher QY due to better passivation from the core-shell structure[13], it will bring more improvements to emission performance by suppressing the spontaneous exciton diffusion and FRET. Apart from the stepped core-shell structure, alloyed structure which adds an intermediate layer between the core and shell material has been studied in recent years.

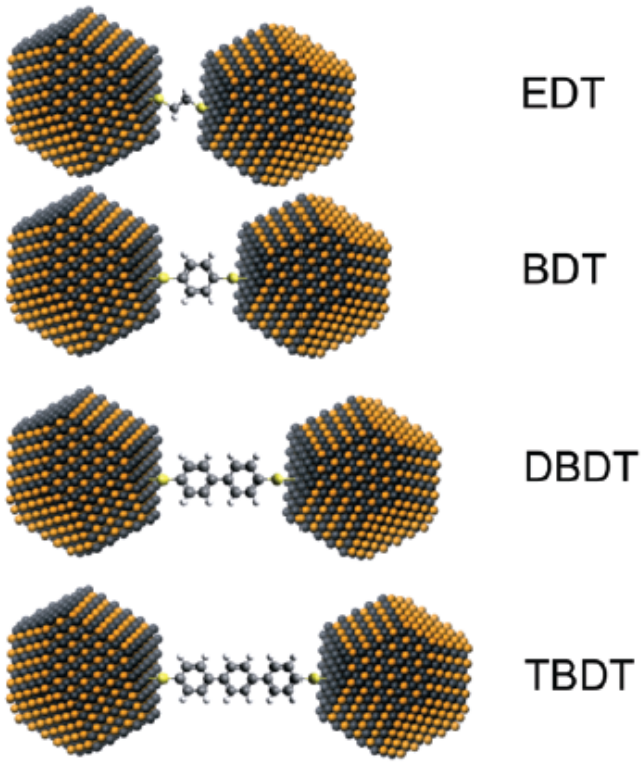

Figure 1.3: [7] Diagram of tuning the inter-dot spacing by capping QDs with different ligands. The organic molecules from top to bottom are ethanedithiol, 1,4-bezenedithiol, 4,4'-dibenzenedithiol and 4,4''-tribenzenedithiol. The inter-dot spacings (not listed)are measured to be 3.0, 3.3, 3.6, 4.0 nm respectively.

This structure has been verified to have even higher quantum yield due to the suppress of Auger recombination [14][15].

Recently, inorganic surface treatments have also been developed and some promising results have been demonstrated [16][17]. In general, inorganic treatments usually replace the oleic acid molecules attached to the Pb atom on the surface by much shorter inorganic - in most cases - halides anions. Such surface modifications are able to enhance the carrier mobility considerably due to much smaller inter-dot spacing, and surprisingly at the same time yield a better emission efficiency. Compared with exchanges with shorter organic ligands such as ethanedithiol(EDT) and mercaptopropionic acid(MPA) which improves charge

transports at the cost of nearly complete quenching of the PL, these inorganic treatments may display great values for application such as solar cells and LED.

1.5 Detailed band edge structures of QDs

The simple picture of radiative recombination between the HOMO and LUMO in a QD whose energy levels can be determined explicitly using all known parameters of bulk lead salts, is an ideal yet not accurate description. There has been quite some evidence showing that even the radiative recombination itself may probably depend on more complex band edge structures. Most related experiments are based on a temperature-dependent PL or transient PL spectrum, which demonstrates a clear absorption or emission peak shift as the temperature changes, which cannot be solely explained by the temperature dependency of bulk bandgap, along with a variation in the peak width and overall PL intensity (Fig.1.4). For CdS/CdSe QDs, two distinct emission peaks of comparable intensity can appear in a wide range of temperature. This is clearly an evidence of the existence of at least two recombination pathways, which can be successfully modeled by a phonon-assisted process regulated by thermodynamics[18]. A two-recombination-pathway model might also explain the PbS/PbSe case in that emission peaks at some specific temperatures appear asymmetric and can be well fitted to two Gaussian peaks [19]. However, no direct evidence that shows two isolated peaks has been provided, and this could otherwise just imply a simple asymmetric distribution of the ensemble of emissions . On the other hand, models have been proposed assuming a continuum of mid-gap emission states [8] to account for the temperature-dependent PL spectra. Interestingly, some claim to have observed a large, phase-transition like redshift in the PL

spectra of thiol-treated PbS [20], and attribute it to the physical state change of QD assemblies brought by the thermal properties of thiols.

The exact nature of lead salt band edge structures is still under investigation. The subtle difference of lattice structures and electron/hole properties between lead salt and cadmium salt may rule out the simple analogy from theories of the latter. These studies may provide solutions to further enhance the performance of elaborate QD-based devices in the future, but are not top relevant given the fact that study of such devices is still in the initial stage and mostly focused on room-temperature performance.

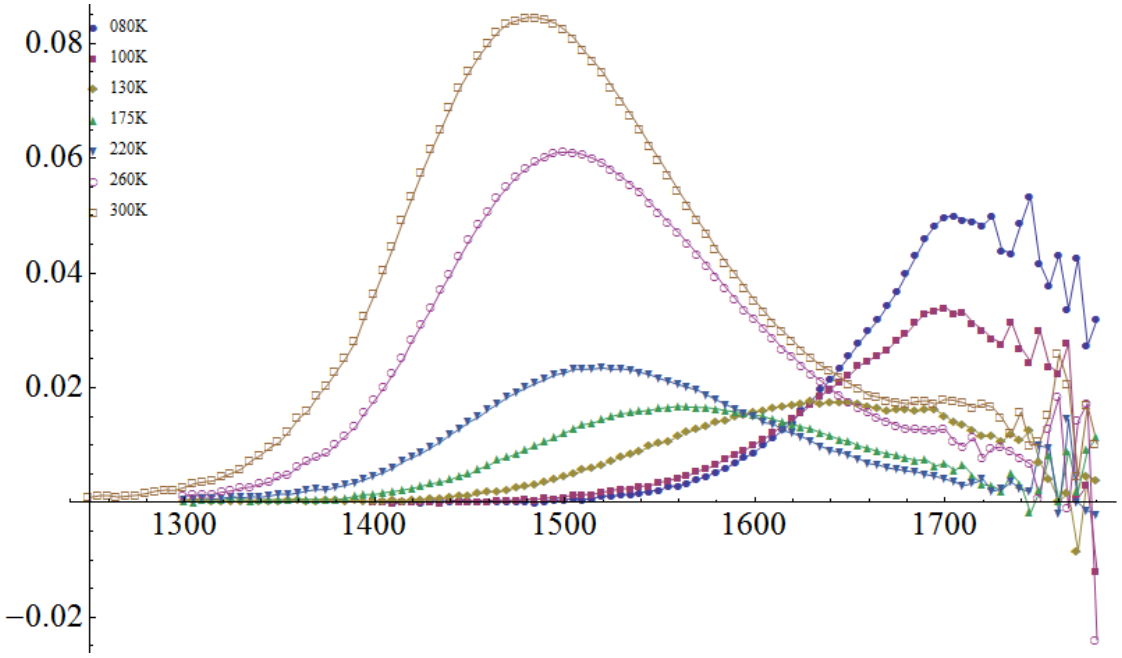

Figure 1.4: Temperature-dependent PL spectra of PbS QDs dispersed in polymer matrix. The horizontal axis refers to wavelength and vertical refers to intensity (a.u.). The noisy tails at higher wavelength are due to detector cut-off. The data clearly shows a trend of blueshift as temperature increases, which may suggest a population flow towards high-energy emissive states.

CHAPTER 2

PRINCIPLES OF QUANTUM DOT LIGHT EMITTING DIODES

2.1 Structure of the device

In an LED, the active region consisting of light-emitting materials is the place where electrons and holes meet and recombine radiatively to emit photons, and in our case, is the solid state PbS QD film. Unlike photoluminescence experiments, where lights get absorbed and hence the creation of electron-hole pairs in individual dots, LEDs require currents, from both electrons and holes, to go through the device under applied voltages and generate excitons. This rationale necessitates a basic structure constituted of QD assemblies, charge transfer layers (CTL) and both electrodes. Based on the principles in section 1.3, charge transfers can be fulfilled by FRET or direct injection from CTL and subsequent diffusion through the QD layer. Thus CTF of both mechanisms can be applied to LEDs (Fig.2.1a). Charge transfers by FRET is usually achieved by employing organic materials which have proved excellent efficiency in applications of biological sensing and OLEDs. The direct injection mechanism is often used for QD LEDs with QD films thicker than one monolayer and in this regime, injection layers are usually made of metal oxides or organic polymers, and specifically, our earlier devices [1][21] have been using poly(3,4-ethylenedioxythiophene) polystyrene sulfonate (PEDOT:PSS) for hole transport layers.

The choices of transfer layers are based on the rationales that carriers injection to(for LEDs) or extraction from(for solar cells) the QD films should be energy-favorable at an equilibrium state or when reasonable voltages are applied. And the fabrication of such layers should be technically cost-effective,

controllable and reproducible. Moreover, mechanisms that hinder leakage current (currents of electrons or holes that go through the whole structure without recombination in active layers) are desirable in order to achieve higher efficiency. One of the first devices using differently doped GaN by energetic neutral atom beam lithography [22], successfully demonstrated direct charge injections into QD layers, however, due to the lack of blocks for leakage current, it only obtained a 1% carrier injection efficiency. Charge injection layers made of ZnO for electrons and PEDOT:PSS for holes solve this problem by providing prohibitive energy barriers for current leakage (Fig.2.1b). It is worth noting that the energy levels of QD layers do not always provide the favorability for charge injections as for smaller dots both band edge levels can lie beyond the levels of corresponding injection layers. This, however, does not bring much difficulty to LEDs because this energy step can always be overcome under forward biases. But there is a requirement, or threshold, for similar-structure-based solar cells, where photogenerated carriers at QD layers must be able to transfer into extraction layers spontaneously to create a photocurrent [23], which sets up the maximum emission wavelength of suitable QDs to be around 900 nm. The materials for electrodes are simply chosen to match the Fermi level of the CTL in order to form Ohmic contacts. ITO, as one of the most widely used transparent conducting materials, is employed in this structure on the light-emitting side for LEDs or entering side for solar cells.

2.2 Surface treatments for QDs

The QDs used either for LEDs or solar cells must go through surface treatments before they are suitable to be integrated into the device. This is because capping

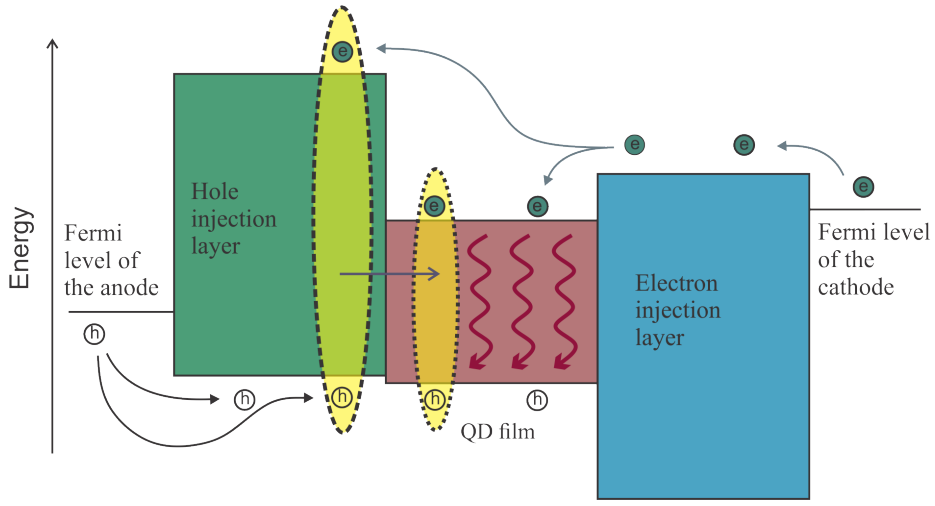

(a) Energy diagram of QD LEDs

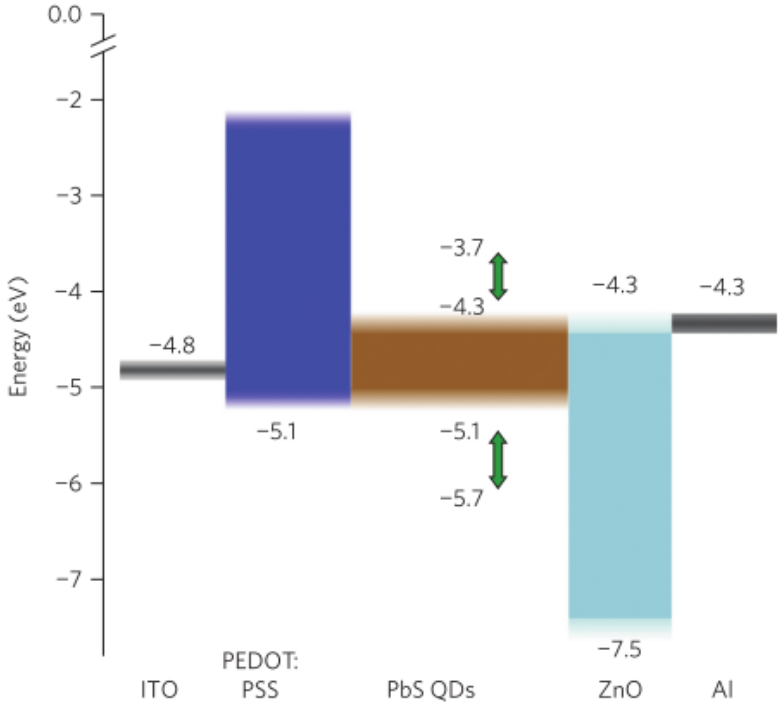

(b) Diagram of the structure we employ

Figure 2.1: Diagrams of QD LED structures. Bands bending are not included here. (a) The structure showing several activities in a working LED. The yellow ellipses denote FRET between the hole transfer layer and the QD layer; (b)[1] The LED with PEDOT:PSS as hole transfer layer and ZnO as electron transfer layer. Energy levels are drawn to scale. Green arrows stand for the tunable range of PbS QDs. Note the barrier at the LUMO of PEDOT:PSS and HOMO of ZnO can effectively stop carriers from penetrating.

ligands oleic-acids on as-synthesized PbS QDs are too long to allow effective carriers transport among the QD ensembles. As is introduced in section 1.4, both organic and inorganic ligand treatments can achieve this purpose, but up to now this is majorly done with organic ligands. Given the fact that shorter linker molecules always facilitate inter-dot charge transfers and is thus desirable for solar cells, the subtlety for LEDs is that charge transfers through exciton dissociation is always accompanied by the sacrifice of the effective radiative recombination. A rough argument is that dissociation gives excitons opportunities to sample more QDs, and thus more traps, which provide them with a higher probability to recombine nonradiatively. For now, the ligands used to treat solar cell QDs are EDT or MPA, both consisting only two -CH_2- with bifunctional groups. On the other hand, the length of organic ligands has an optimum point where charge transfer and radiative efficiency are balanced [1]. Our group reached the maximum external quantum efficiency (EQE) for LEDs with mercaptooctanoic acid(MOA) treated PbS QDs, corresponding to an inter-dot spacing of 6.3 nm. The rate of carrier transfers in this regime is believed to only depend on the length of the molecule, and little related to the specific atoms or function groups. For this reason, we include both MOA and octanedithiol (ODT) in the list of treatments. The other ligands in use are Hexanethiol (HT), Octanethiol (OT), MHA, and hexanedithiol(HDT).

CHAPTER 3

EXPERIMENT METHODS, RESULTS AND ANALYSES

3.1 Fabrication processes of devices and test setup

The exact structure of LEDs we fabricated and studied for this thesis is slightly different from what is illustrated in the last chapter. First, in order to realize a full inorganic structure (except for the capping ligands), we employed NiO as the hole injection layer to replace the PEDOT:PSS [23], which has a valance band level around -5.3 eV and conduction band level around -1.5 eV, similar to those of PEDOT:PSS but with a slightly higher barrier for electrons. Also we switched the order of two injection layers and thus ITO contacts ZnO, and to match the Fermi level of the hole injection layer NiO, gold was selected for the anode. This order of layers, often called the "inverted structure", was believed to give a better performance because ITO, as a naturally n-doped material, should be more suitable for electron injections.

The syntheses of PbS QDs follow the procedures reported in ref.[24]. The as-synthesized QDs are washed at least three cycles by dissolving in hexane , precipitation with acetone, centrifugation at 4.4 rpm for 3 minutes, and discarding of the supernatant. The QDs are then dried in nitrogen, and subsequently dissolved in hexane to form the solution of certain concentration, usually at 30 mg/ml.

The deposition starts on pre-patterned ITO substrates. The substrates are cleaned by DI-water, acetone and isopropanol(IPA) in sequence with sonicators. In order to have a precise control of the thickness and good quality of

charge injection layers, we utilize sputtering to produce these layers. The ZnO deposition is done first. The recipe follows the one from ref[23]. The sputtering is conducted with a zinc target under room temperature, in the mixture of Ar and O_2 with pressure ratio $4:1$ and a total pressure at 5 mtorr with substrates sitting on the rotating stage to provide a uniform coverage. Generally, the ZnO layer is deposited to 15-30 nm. There is an optimum thickness, 20 nm, for the same-structure-based solar cells. However, without more detailed reasoning why this should be the best thickness for LEDs, we still choose it for our devices. The deposited ZnO film appears with great transparency with only a very slight tint, and uniformity when looked by eye.

PbS QDs deposition and following treatments are carried out on the ZnO covered substrates with spin-coating. Firstly, 200 μl , 30 mg/ml PbS hexane solution is dropped onto the substrate with a pipette and spun for 30 s at 1000 rpm. The film is then treated with 1 ml solution (0.1 M in acetonitrile) of organic ligands for ligand exchanges by dripping the solution on the PbS film, waiting for 1 min to allow complete reactions and spinning for 30 s. After that, 1 ml acetonitrile at a time is dispensed on top of the film to rinse it with the substrate spinning, which is repeated 5 times to ensure the complete removal of free molecules. This whole procedure constitutes one cycle of deposition and treatment. Usually three cycles are performed to make a 100-200 nm thick film, which is the protocol used in ref[1][21][23]. After the QD deposition, the NiO film is then coated on the top by sputtering. The pressure ratio of Ar to O_2 is now set to $99:1$ at a total pressure of 10 mtorr. The thickness is controlled to be around 10 nm. But sometimes to ensure a crackless coverage on rough QD film surfaces, thicker NiO film is deposited (10-40 nm). The fabrication is finalized by deposition of 60 nm-thick gold electrodes with a mask by thermal

evaporation.

As for characterization of the device, Lakeshore full wafer cryogenic probe system is used to measure the current-voltage relations. Electroluminescence and EQE measurements are conducted using a Keithley source meter (236 and 2400) to provide and monitor currents. There are two test setups (Fig.2.2), the first using a ThorLab PM100D powermeter with an IR photodiode positioned at a certain distance perpendicularly to the emitting surface of LEDs. The total emission power is calculated with known geometry (distance, size of the sensor and solid angle subtended by the detector) assuming Lambertian emission. The second method uses a ThorLab integrating sphere to collect all emitted power to be measured by a calibrated UDT Instrument S370 optometer. The EL and PL spectra are obtained with a Princeton Instruments SP2300 monochromater and infrared detectors. The excitation for PL comes from a 400 nm laser diode.

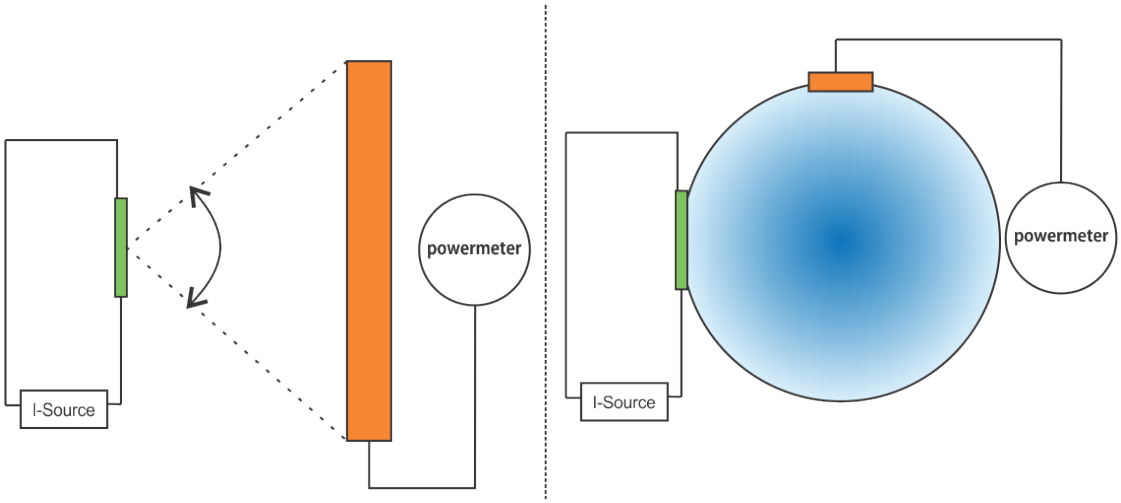

Figure 3.1: Two different setups for EL measurements (green for the LED pixel, orange for the photodetector, blue for the integrating sphere): the left requires the geometry details and accurate positioning in order to calculate the emitted power; the right uses an integrating sphere to collect all the light.

3.2 Experiment results

3.2.1 Measured properties of films

To ensure that the fabrication process provides the oxide layers and QD films with quality and thickness as expected, we measured some of the physical properties including crystallinity and transparency of the oxide films and thickness and surface roughness of PbS QD films.

The crystallinity of ZnO and NiO films were measured with X-ray Diffractometer (XRD) in the 2θ regime. The peaks denoting the specific diffracted signals of a plane are shown in Fig.3.2a. The data reveals good crystallinity of both sputtered films. It is worth noting that the 2θ setup is designed to work with powder samples and signals can be hard to collect for film samples, however, fair intensities of only a few visible peaks in the figure imply the precise orientation of the films with respect to the substrate, and large domains in the film maintaining a uniform lattice, especially for ZnO film where only derivatives of a particular direction (002) can be seen. The transparency characterized by transmittance of the same films for XRD, was measured using the Shimadzu spectrometer (Fig.3.2b). Both films have great transmittance (80-90%)for light from 1800 nm all the way down to the band edge absorption, which indicates their desirability for light extraction.

Measurements of the surface profile of PbS films was conducted by Veeco Dimension 3100 ambient AFM. Films of different treatments and different numbers of cycles of depositions on ZnO coated glass substrates were measured, which were exactly the way they would be in LEDs. See Fig.3.3 and Table 3.1.

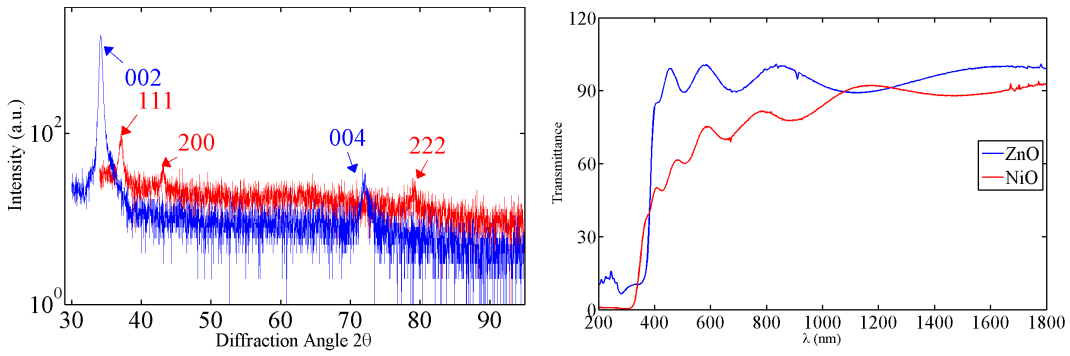

(a) (b)

Figure 3.2: XRD spectra and transmittance measured of ZnO (410 nm) and NiO (610 nm) films. The ZnO XRD shows two distinct peaks without any other discernible signals , 002 and 004, both related to one orientation. The NiO film spectrum displays three peaks, however, the 200 one is not the derivative of the other two, which indicates the existence of multi-orientation w.r.t. to the substrate.

The results confirmed the 100-200 nm thickness and good surface smoothness by deposition methods described in section 2.1. However, a three-cycle spin coating with 30 mg/ml PbS solutions, according to the results here, always led to a film well thicker than 100 nm rather than close to 100 nm. Thus in order to produce films around 100 nm, one needs to adjust the concentration or spin speed. That being said, the exact differences besides thickness, between films deposited from different number of cycles and moreover, the apparent and underlying relations between film thickness and LED performance, still require more investigation.

These characterizations of the basic physical properties of each film prove to us the abilities of corresponding methods to produce films of great quality in a well controlled manner.

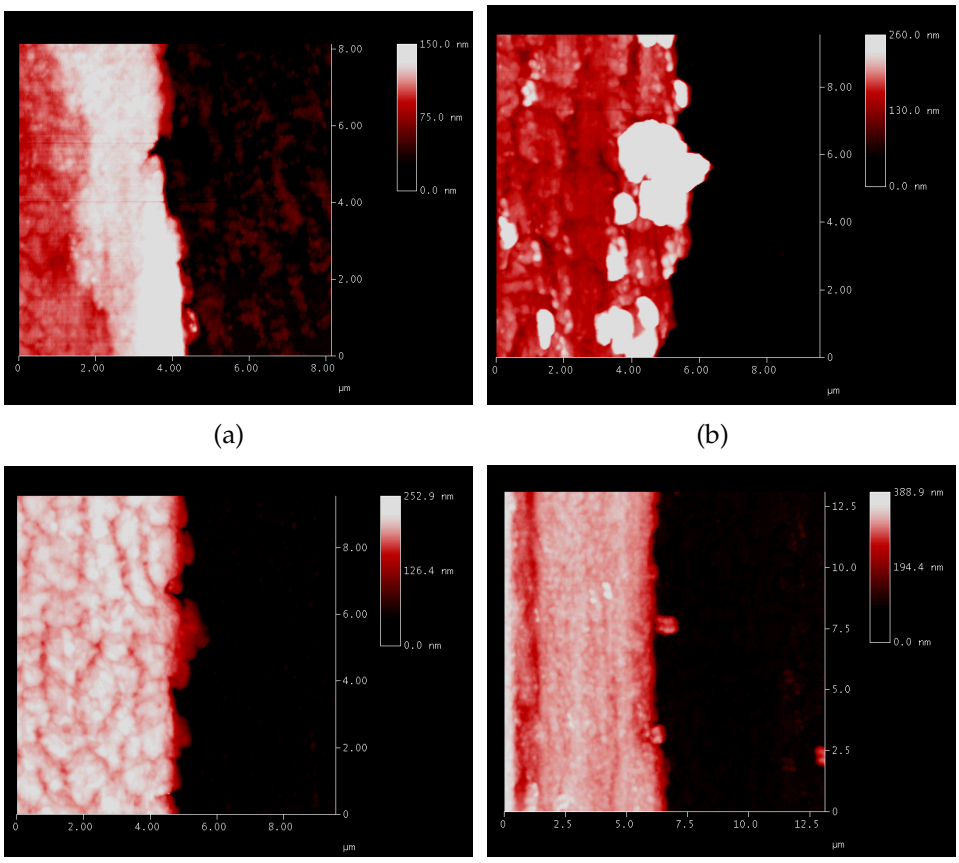

(a) (b)

(c) (d)

Figure 3.3: AFM images of PbS films from depositions of different numbers of cycles. one cycle (a); two cycles (b) ; three cycles (c); four cycles (d).

	one cycle	two cycles	three cycles	four cycles
ammonium sulfide + iodine			215 nm	
EDT + iodine	75 nm (18 nm)		155 nm (13 nm)	
ODT	82 nm (9 nm)	118 nm (11 nm)	171 nm (9 nm)	240 nm (15 nm)

Table 3.1: The thickness of films. The values in parentheses refer to the roughness of the film. It is evident here that the total thickness is not necessarily proportional to the total number of cycles, and the roughness is almost independent of the total thickness but may be related to the type of treatment.

3.2.2 Current-Voltage curves, efficiency and radiance of the devices

Before showing the current-voltage relations of LEDs, we need to first specify two different patterns of the devices we fabricated. See Fig.3.4. These two patterns correspond to two different setups we mentioned in section 3.1. The procedures of fabrication are exactly the same for both, except different evaporation masks are used.

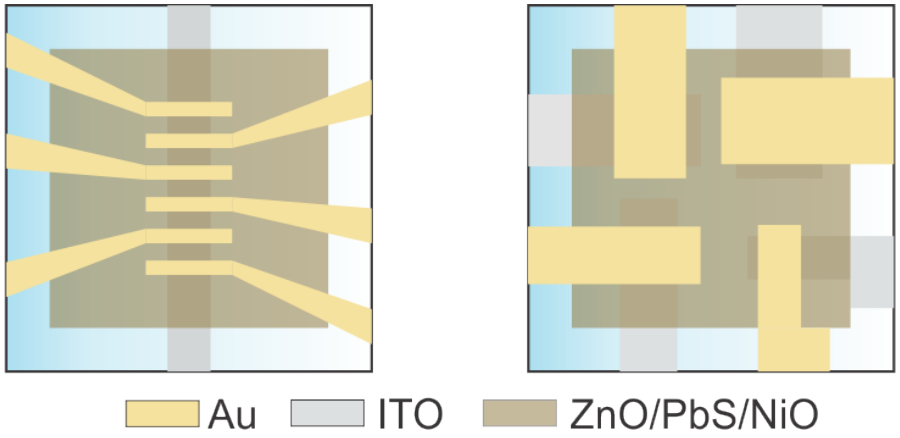

Figure 3.4: Two different layouts of the device. The left pattern consists of 6 identical pixels each with a 1×3 mm^2 active area, while the other have four different size of pixels with areas 3×3 mm^2, 4×4 mm^2, 5×5 mm^2 and 6×6 mm^2 respectively.

The I-V curve is shown here in Fig.3.5, measured on a 3×3 mm^2 pixel of a hexanethiol treated device of the second pattern in Fig.3.4. There is a clear rectification behavior and a small leakage current under reverse biases. The positive current starts to increase significantly beyond 1 V, which is proposed to be the "built-in potential" of the device and is dependent on the energy offset between QD and charge injection layers [1]. Fig.3.5(b) shows the I-V relation with built-in potential (1.1V) subtracted . The nearly constant slope at higher

injection level reveals a single operation regime. Although the voltage only reaches 2 V in the figure, we were able to apply as high as 7 V to the pixel where 90 mA current was yielded, corresponding to 1 A/cm^2 density.

As for the efficiency and radiance, however, the hexanethiol treated device did not exhibit a remarkable performance. The EQE is under 0.02% over a wide current range from 5 mA to 100 mA. At 50 mA, which is 0.56 A/cm^2, the measured total power output is 7.8 μW, which yields a 0.015% EQE and 0.28/W/sr/m^2 radiance. The EL spectrum peaks at 1200 nm, the comparison between EL and PL is shown in Fig.3.6.

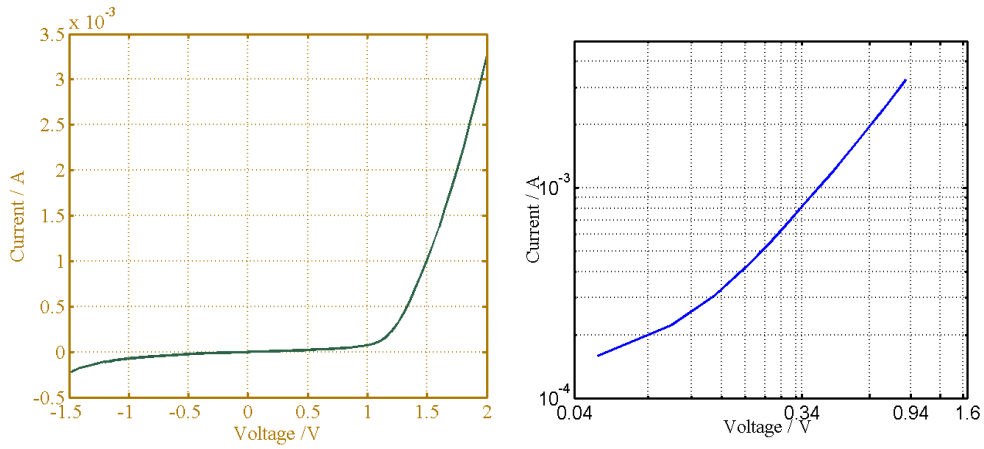

(a) (b)

Figure 3.5: Current-voltage relation of the pixel. The linear graph (a) indicates a turn-on voltage around 1.1 V while the logarithm graph (b) exhibits a nearly constant slope.

The low luminescence of the device probably comes from the comparatively arbitrary choice of ligands exchange, which should usually be conducted with bilinker molecules with function groups on both sides (MOA and ODT) rather than monolinker molecules. That being said, these device still bears the merit of high conductance which allows a considerably high current density at a reasonably low voltage, and this further confirms the capability of current injection of

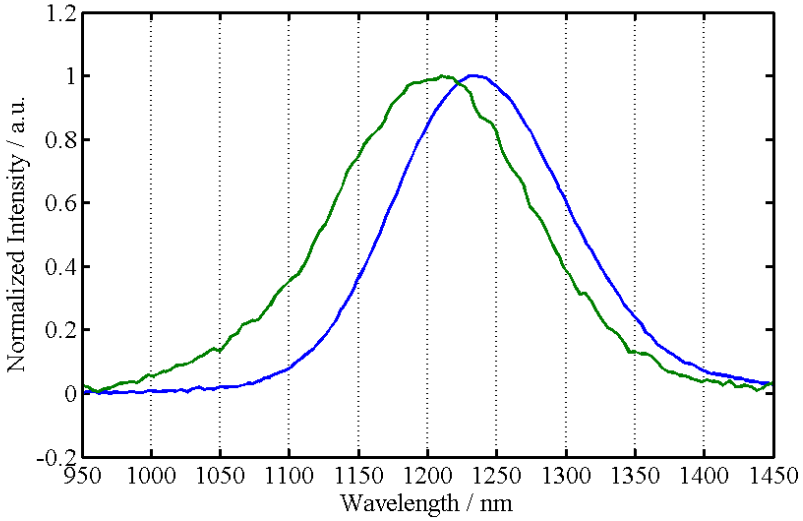

Figure 3.6: Photoluminescence (blue) and electroluminescence (green) spectrum of the hexanethiol treated device. treated device. A small blue shift is observed from PL to EL.

such structures.

The subsequent LEDs were fabricated with various combinations of PbS QDs with emission 1100 nm -1500 nm and MHA,MOA,HDT and ODT treatments. We had experienced some difficulty in making devices with consistent performance, especially for pixels from different batches, even if all the fabrication recipes and parameters were controlled unchanged, individual behaviors could vary substantially. Moreover, few of the devices exhibited conspicuous enhancements despite that various adjustments, which were expected to bring about significant improvements to the performance, were attempted . Also the underdeveloped test setup had induced large uncertainty during the measurements. These facts prevented most direct comparisons between devices with adjusted parameters, and made it difficult to conclude whether a variation in the performance, if any, resulted from the exact adjustment in the fabrication process or was simply due to the hysteresis of everything involved.

Nonetheless, based on the optimum choice of QD size, layer thickness and ligands treatment of previous achievements [1][25] on PbS LEDs, we still fabricated several devices following the same conditions, and the best devices of all, though unable to compare those reported previously, indeed came from the ones using MOA/ODT treated films with emission at 1000-1200 nm. The first batch of devices with ODT treated films and 1500 nm emission was able to achieve a 0.042% efficiency and a radiance 0.57 $W/sr/m^2$ at 0.14 A/cm^2 and 4.6 V. The EQE might possibly be higher at lower current density if the luminescence was measured throughout a wider current range, but this was not fulfilled due to the difficulty by experiment setup. This improvement from the hexanethiol treated device was not distinct as expected in its extent though, according to the supplementary information of ref[1], the best efficiency achieved from QDs with emission around 1500 nm was also only 0.04%, so in this case, the ODT treated device actually reached the previous standard. Based on the data that replacing larger QDs (1500 nm in emission) with smaller QDs (1100 nm in emission) could result in a more than tenfold increase in the maximum EQE, we produced devices with emission around 1150 nm under the same treatment with ODT. The result was a little disappointing in that only a twofold increase in the EQE was observed. This time the pixel was tested in the second setup of Fig.3.1 and a current sweep was carried out. See the curve in Fig.3.7. The highest measured EQE reached nearly 0.1 %. However, during the measurement the device behaved quite abnormally in that at a constant current level, it would suddenly switch to another "state" that the conductance immediately rose up , as manifested by a dramatic drop in the voltage, accompanied by the complete quenching of the EL. This could be fixed temporarily by tuning the current back and forth and returning to the desired level, or by switching off the power for

a while and then switching on. But the device would always stay in this undesired state at current levels out of the range in Fig.3.7. This eccentricity had not occurred for devices tested earlier. On the other hand, it is worth noting that the achievable current density was much lower than that of the device mentioned above, in fact, the highest current density, 0.18 A/cm^2, was obtained at an unusually high voltage, 18 V. In addition, MOA treated devices had less chance to function properly and for those working devices, the numbers were no better than those of the ODT treated ones.

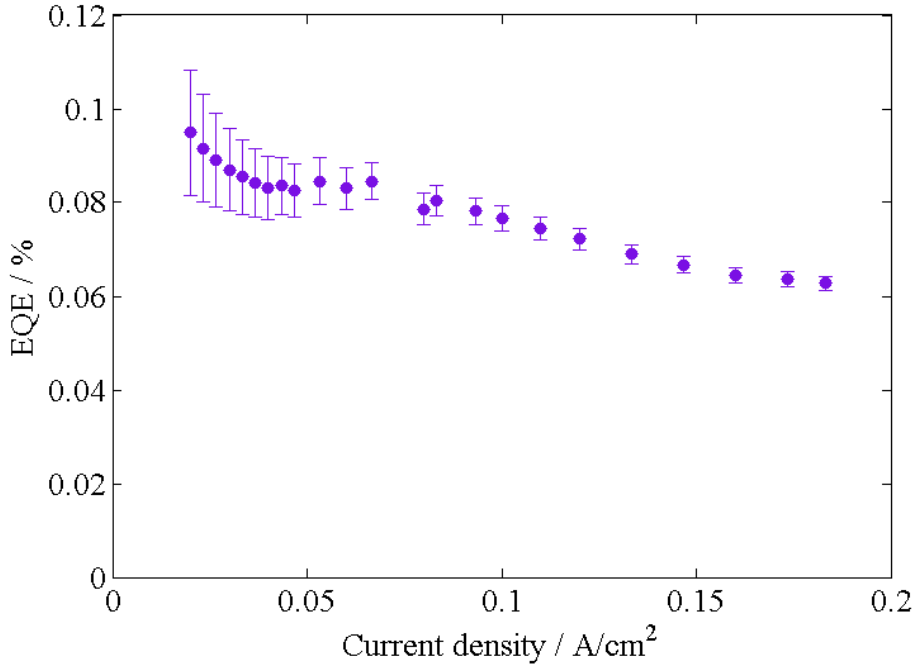

Figure 3.7: EQE and current density relation of the measured pixel. Complete behavior of the curve could not be discovered because of the failure to maintain the normal operating state.

Treatment	Size $(mm)^2$	WL (nm)	Radiance $(W/sr/m^2)$	EQE (%)	Current & voltage reached	Swept to find the maximum EQE ?
HT	3x3	1200	0.28 (56 mA, 3.7V)	0.015	160 mA, 9.5V	No
MHA	5x5	1500	0.18 (50 mA, 3.3V)	0.027	-	No
ODT	3x3	1500	0.57 (50 mA, 4.6V)	0.042	120 mA, 9.8 V	No
MOA	1x3	1400	-	0.058	7 mA, 5.3 V	No
ODT	1x3	1160	0.36 (5.5 mA, 16.7V)	0.096	5.5 mA, 16.7V	Yes

Table 3.2: Summary of functioning LED pixels. The radiance and EQE were measured under the same current and voltage in the parentheses; Pixels labeled "No" in the last column suggest the possibility to find higher EQE if they were to be tested with current sweeps.

3.3 Analysis on experiment results

Table.3.2 summarizes the performance of various devices tested. It suggests approximately that ligands with eight carbon atoms and bi-functional groups and QDs with emission around 1100 nm might perform better as LEDs. But convincing arguments cannot be made due to the lack of sufficient functioning devices. For now, it can be confirmed that the structure with both inorganic injection layers is capable of providing enough carriers into the QD layer. The conductance of most devices is relatively high to allow current density up to 1 A/cm^2 within the safe voltage range. We would like to point out that the characteristic of most malfunctioning devices is the concurrence of unexpected high current (abnormally high conductance) and undetectable electroluminescence. If this is because of current leakage, it is confusing and worth investigating the

origin and its relationship with the effective current for recombination. And it is always true that the efficiency of luminescence depends largely on the recombination behaviors of the QDs themselves under the condition of electrical injection of carriers. We will proceed with relevant discussions in the next chapter. One more thing to point out is the good air stability and resistance to aging of the LEDs. Though accurate records are not kept, performance of most devices still stay roughly at the same level or underwent a negligible degradation after prolonged exposure (1-4 months) in ambient air.

CHAPTER 4

DISCUSSION AND FUTURE DIRECTIONS

4.1 Interrelations between mechanisms of efficiency loss in QD LEDs

Just as the power conversion efficiency of solar cells, the EQE of LEDs has always been one of the major concerns, especially for newly developed devices, such as QD LEDs. A relatively comprehensive understanding of various mechanisms in an operating QD LED is yet to be achieved. Most explanations regarding the efficiency of LEDs are based upon isolated studies involving only part of the device structure. With little knowledge of connections between these factors and their relative importance on the performance of LEDs, most in general believe that three of the main reasons for efficiency loss in QD LEDs are carrier trapping, Auger recombination and field-induced quenching. However, except the last one, these factors are not unique to LEDs in that the PL behavior of QDs are also influenced by them. As the QY of PbS QD solutions has reached as high as 80% [19], such mechanisms alone cannot satisfactorily explain the order-of-magnitude lower efficiency in LEDs. If they really have strong impacts on the radiative behavior of QDs, it is the underlying reason, which makes these processes much more dominant in devices, that should draw more attention. Here we propose that this reason could possibly be the local and instant carrier imbalance on single QDs, which is the absence of its counterpart of a carrier in one single QD at a specific time period. Unlike the time-averaged carrier concentration imbalance in QD ensembles, which cannot appear in a charge-free and undoped region, the local instant imbalance can occur at any site once charge

diffusion is allowed or electrical injection exists. This is simply because time-average does not mean constant throughout the time. The fluctuation in the carrier number of a single dot can create the imbalance instantly between electrons and holes, and thus allow different occupancy state, for a short moment.

To be more specific, the effect of this imbalance would mostly take place when its duration is comparable to or longer than the recombination pathways allowed by the corresponding state. This can possibly explain the large efficiency loss and lifetime drop when QD solution is made into compact films when exciton dissociation is facilitated. Consider the case where a QD with one exciton sits near a QD at ground state, if an electron diffuses into the second QD, creating two imbalanced QD at this moment, both extra carriers (hole on the first QD and electron on the second) may then transit into the trap of their own sites. Note at this given instant, radiative recombination is forbidden due to the lack of the counterpart of carriers. And if they are trapped and the imbalance is subsequently compensated for by following carrier diffusions, the net effect is one exciton energy loss nonradiatively without affecting the long-timescale charge balance. Certainly this process is stochastic and it may probably not proceed this way, but the existence of a short term imbalance creates the situation where trapping is the only viable pathway for carriers, and thus increases the overall probability of trapping, compared with recombination in isolated QD ensembles, which always competes between trapping and emission and both are allowed probabilistically with respect to their rates.

This reasoning also applies to the instant increase in the chance for Auger recombination. The randomly diffused single carrier for one single exciton QD will create two charged exciton state, upon its landing on the other single exci-

ton QD, and thus allows nonradiative recombination. And the time-averaged state of both QDs involved can still be strict single exciton, which apparently forbids Auger recombination. A more interesting speculation would be that even if all QDs have no traps at all, i.e., with exactly 100% QY when uncoupled, they could still suffer from nonradiative loss when made into compact ensembles due to the emerging events of Auger recombination.

Moreover, LEDs operate differently from PL experiments in that carriers are pumped into QDs electrically from different directions, unlike excitons are always created simultaneously with equal number of electrons and holes upon absorption in PL. This fact may simply lead to much more occurrences of instant imbalance compared with QD ensembles of exactly equivalent concentration of both carriers in PL experiments, and therefore causes more efficiency drop. In most cases, the estimated average concentration of carriers per QD is well below one which apparently indicates the negligibility of Auger recombination, but with instant carrier imbalance considered, Auger recombination becomes a possible pathway for efficiency loss.

Thus, instant carrier imbalance actually strengthens the negative impacts of trapping and Auger recombination on LED efficiency. Moreover, the carrier distribution in a full device can be more complicated by the band alignment between different layers of unintended doping of the QDs, which would even break the time-average balance between carriers. In fact, the whole picture of carrier dynamics through the entire QD film in a device can be extremely intricate where charge injections, exciton dissociations, FRET and recombinations are all involved, coupled and interrelated. There is almost no convenient way to describe it with only statistical parameters, and difficult to estimate how much

each factor, including the instant imbalance, really takes effect. Though models have been proposed to describe the single type carrier transfer inside the QD layer as an analogy to bulk transfer [12][26], the detailed processes are still not fully accounted for. In order to get an overall accurate and comprehensive description of carrier lifetimes, current density distributions and emission efficiencies, we might need to resort to Monte Carlo simulations [27].

4.2 More thoughts regarding the efficiency droop in LEDs

LEDs are subject to an additional efficiency loss when the applied voltage gets higher, which is usually referred to as efficiency droop. One of the mechanisms is proposed to be the field-induced quenching, results from the spatial separation of electron and hole wavefunctions under large electric field, and has been proved to exist in QD LEDs operated at high voltages [28]. But for practical devices in our case, the voltage required to induce such effect is so high (1.5 MV / cm , corresponding to 15 V applied directly on the PbS QD film solely) that it probably would not be a concern at the moment. On the other hand, high voltage can also cause leakage current flowing through the device without recombination in the active layer. Though it can be easily understood that the possibility and occurrence of leakage strongly depends on the exact structure of the device, the exact dependence and quantitative relations are yet to be discovered. Moreover, an ineffective charge barrier in the structure can cause leakage even at low applied voltages. Recall the abnormality of the device we measured with a high conductance suddenly arising, which can be quite likely the characteristic behavior of leakage current. However, the complete quenching of the EL accompanying this leakage is hard to understand because leakage current,

usually modeled by a short circuit, should not suppress the effective current for recombinations. Also the fact that this structure succeeded in blocking carriers in some devices while failed for others might complicates the initially simple picture of charge barriers for leakage. It is therefore necessary to investigate more into this structure and look for some possible improvements.

4.3 Future directions

The development of PbS / PbSe QD LEDs, honestly, is not keeping up with its counterpart in visible range, CdSe / CdS LEDs, which have already achieved an EQE as high as 18% [29]. Bearing in mind the considerable differences in band structures between these two types of QDs though, there is no fundamental limit for PbS QD LEDs to achieve higher performance from the present level. As the photoluminescence quantum yield of the QD ensemble is always the essential factor to determine the overall quality of its photogeneration-related behaviors, a great number of efforts have been made towards obtaining higher PL QY. Most techniques are aimed at producing better surface passivation of QDs, as is introduced in section 1.4. Core-shell structure is one of the most eligible techniques in reaching this purpose. As for CdSe/CdS QDs, apart from considerably reducing surface traps and enhancing radiative recombination efficiency by attaching many layers of shell materials [13], novel structures such as alloyed core-shell QD are able to not only reduce traps, but also increase the radiative Auger recombination efficiency of charged QDs [14]. Moreover, only a thin layer of alloyed shell is required, so this improvement can be attained without sacrificing the mobility of carriers due to extended inter-dot spacing by traditional core-shell structure. The alloyed shell technique has also been

realized for PbS/PbSe based QDs [19], and may be soon applied to devices.

Inorganic treatments by halide molecules have been explored recently. The surface capping by much smaller halide atoms is reported to produce better passivation as well as closer inter-dot distance at the same time. We have also succeeded in producing thin PbS QD films showing both better PL intensity than OA films and easier carrier transfer due to closer inter-dot distances. This technique is yet to be refined to produce more controllable and consistent result for thicker QD films suitable for LEDs. Compared to core-shell structure, halide surface passivation gives more freedom for the choice of ligands and more convenience from the post-processing method.

However, before seeking more innovations in QDs themselves, it is critical to make the best of the present LED structure and ensure that it functions as expected in terms of effectively injection of carriers. Otherwise the failure in the structure, such as current leakage, may simply leave the QDs helpless regardless of their QY. More understandings and some necessary adjustments may be demanded for the successful operation of the structure.

BIBLIOGRAPHY

[1] L. Sun, J. J. Choi, D. Stachnik, A. C. Bartnik, B. R. Hyun, G. G. Malliaras, T. Hanrath, and F. W. Wise. Bright infrared quantum-dot light-emitting diodes through inter-dot spacing control. *Nat Nanotechnol*, 7(6):369–73, 2012.

[2] Inuk Kang and Frank W Wise. Electronic structure and optical properties of PbS and PbSe quantum dots. *J.Opt.Soc.Am.B*, 14(7):1632–1646, 1997.

[3] Frank W. Wise. Lead salt quantum dots: the limit of strong quantum confinement. *Accounts of Chemical Research*, 33(11):773–780, 2000.

[4] Zhonghua Yu, Jingbo Li, Donald B O'Connor, Lin-Wang Wang, and Paul F Barbara. Large resonant Stokes shift in CdS nanocrystals. *The Journal of Physical Chemistry B*, 107(24):5670–5674, 2003.

[5] Victor I. Klimov. Optical nonlinearities and ultrafast carrier dynamics in semiconductor nanocrystals. *The Journal of Physical Chemistry B*, 104(26):6112–6123, 2000.

[6] S. Schmitt-Rink, D. Miller, and D. Chemla. Theory of the linear and nonlinear optical properties of semiconductor microcrystallites. *Physical Review B*, 35(15):8113–8125, 1987.

[7] J. J. Choi, J. Luria, B. R. Hyun, A. C. Bartnik, L. Sun, Y. F. Lim, J. A. Marohn, F. W. Wise, and T. Hanrath. Photogenerated exciton dissociation in highly coupled lead salt nanocrystal assemblies. *Nano Lett*, 10(5):1805–11, 2010.

[8] J. Gao and J. C. Johnson. Charge trapping in bright and dark states of coupled PbS quantum dot films. *ACS Nano*, 6(4):3292–303, 2012.

[9] J. A. McGuire, M. Sykora, J. Joo, J. M. Pietryga, and V. I. Klimov. Apparent versus true carrier multiplication yields in semiconductor nanocrystals. *Nano Lett*, 10(6):2049–57, 2010.

[10] Stephen W Clark, Jeffrey M Harbold, and Frank W Wise. Resonant energy transfer in PbS quantum dots. *The Journal of Physical Chemistry C*, 111(20):7302–7305, 2007.

[11] CR Kagan, CB Murray, M Nirmal, and MG Bawendi. Electronic energy

transfer in CdSe quantum dot solids. *Physical Review Letters*, 76(9):1517, 1996.

[12] David Zhitomirsky, Oleksandr Voznyy, Sjoerd Hoogland, and Edward H Sargent. Measuring charge carrier diffusion in coupled colloidal quantum dot solids. *ACS nano*, 7(6):5282–5290, 2013.

[13] B. N. Pal, Y. Ghosh, S. Brovelli, R. Laocharoensuk, V. I. Klimov, J. A. Hollingsworth, and H. Htoon. 'Giant' CdSe/CdS core/shell nanocrystal quantum dots as efficient electroluminescent materials: strong influence of shell thickness on light-emitting diode performance. *Nano Lett*, 12(1):331–6, 2012.

[14] Y. S. Park, W. K. Bae, L. A. Padilha, J. M. Pietryga, and V. I. Klimov. Effect of the core/shell interface on Auger recombination evaluated by single-quantum-dot spectroscopy. *Nano Lett*, 14(2):396–402, 2014.

[15] X. Wang, X. Ren, K. Kahen, M. A. Hahn, M. Rajeswaran, S. Maccagnano-Zacher, J. Silcox, G. E. Cragg, A. L. Efros, and T. D. Krauss. Non-blinking semiconductor nanocrystals. *Nature*, 459(7247):686–9, 2009.

[16] Jiang Tang, Kyle W Kemp, Sjoerd Hoogland, Kwang S Jeong, Huan Liu, Larissa Levina, Melissa Furukawa, Xihua Wang, Ratan Debnath, Dongkyu Cha, et al. Colloidal-quantum-dot photovoltaics using atomic-ligand passivation. *Nature materials*, 10(10):765–771, 2011.

[17] Guangda Niu, Liduo Wang, Rui Gao, Beibei Ma, Haopeng Dong, and Yong Qiu. Inorganic iodide ligands in ex situ PbS quantum dot sensitized solar cells with I-/I 3- electrolytes. *Journal of Materials Chemistry*, 22(33):16914–16919, 2012.

[18] Jonathan Mooney, Michael Krause, Jonathan Saari, and Patanjali Kambhampati. Challenge to the deep-trap model of the surface in semiconductor nanocrystals. *Physical Review B*, 87(8), 2013.

[19] Efrat Lifshitz, Georgy I Maikov, Roman Vaxenburg, Diana Yanover, Anna Brusilovski, Jenya Tilchin, and Aldona Sashchiuk. Temperature-Dependent optical properties of polloidal IV-VI quantum dots, composed of core/shell heterostructures with alloy components.

[20] C. A. Nelson and X. Y. Zhu. Reversible surface electronic traps in PbS quantum dot solids induced by an order-disorder phase transition in capping molecules. *J.Am.Chem.Soc*, 134(18):7592–5, 2012.

[21] J. J. Choi, Y. F. Lim, M. B. Santiago-Berrios, M. Oh, B. R. Hyun, L. Sun, A. C. Bartnik, A. Goedhart, G. G. Malliaras, H. D. Abruna, F. W. Wise, and T. Hanrath. PbSe nanocrystal excitonic solar cells. *Nano Lett*, 9(11):3749–55, 2009.

[22] A. H. Mueller, M. A. Petruska, M. Achermann, D. J. Werder, E. A. Akhadov, D. D. Koleske, M. A. Hoffbauer, and V. I. Klimov. Multicolor light-emitting diodes based on semiconductor nanocrystals encapsulated in GaN charge injection layers. *Nano Lett*, 5(6):1039–44, 2005.

[23] Byung-Ryool Hyun, Joshua J Choi, Kyle L Seyler, Tobias Hanrath, and Frank W Wise. Heterojunction PbS nanocrystal solar cells with oxide charge-transport layers. *ACS Nano*, 7(12):10938–10947, 2013.

[24] Margaret A Hines and Gregory D Scholes. Colloidal PbS nanocrystals with size-tunable near-infrared emission: observation of post-synthesis self-narrowing of the particle size distribution. *Advanced Materials*, 15(21):1844–1849, 2003.

[25] Xin Ma, Fan Xu, Jaime Benavides, and Sylvain G Cloutier. High performance hybrid near-infrared LEDs using benzenedithiol cross-linked PbS colloidal nanocrystals. *Organic Electronics*, 13(3):525–531, 2012.

[26] D. Zhitomirsky, O. Voznyy, L. Levina, S. Hoogland, K. W. Kemp, A. H. Ip, S. M. Thon, and E. H. Sargent. Engineering colloidal quantum dot solids within and beyond the mobility-invariant regime. *Nat Commun*, 5:3803, 2014.

[27] Chris Groves. Developing understanding of organic photovoltaic devices: kinetic Monte Carlo models of geminate and non-geminate recombination, charge transport and charge extraction. *Energy & Environmental Science*, 6(11):3202, 2013.

[28] Yasuhiro Shirasaki, Geoffrey J Supran, William A Tisdale, and Vladimir Bulović. Origin of efficiency roll-off in colloidal quantum-dot light-emitting diodes. *Physical review letters*, 110(21):217403, 2013.

[29] Benjamin S Mashford, Matthew Stevenson, Zoran Popovic, Charles Hamilton, Zhaoqun Zhou, Craig Breen, Jonathan Steckel, Vladimir Bulovic, Moungi Bawendi, Seth Coe-Sullivan, et al. High-efficiency quantum-dot light-emitting devices with enhanced charge injection. *Nature Photonics*, 7(5):407–412, 2013.